Title

A fractal model of granitic intrusion and variability based on cellular automata

Authors

Xiong, Yihui
Zuo, Renguang
Clarke, Keith C

Publication Date

2019-08-01

DOI

10.1016/j.cageo.2019.05.002

Peer reviewed

Computers & Geosciences 129 (2019) 40–48

Contents lists available at ScienceDirect

Computers and Geosciences

journal homepage: www.elsevier.com/locate/cageo

Research paper

A fractal model of granitic intrusion and variability based on cellular automata

Yihui Xiong [a,b], Renguang Zuo [a,*], Keith C. Clarke [b,**]

[a] State Key Laboratory of Geological Processes and Mineral Resources, China University of Geosciences, Wuhan, 430074, China
[b] Department of Geography, University of California, Santa Barbara, CA, USA

ARTICLE INFO

Keywords:
Magma ascent
Granitic intrusions
Cellular automata
Fractal model
Self-organized criticality

ABSTRACT

Among the various mechanisms for magma ascent and emplacement, rock fracturing is a highly significant factor. In this study, a cellular automaton based on the Olami-Feder-Christensen model was used to generate a self-organized network in which magma can ascend and be arrested to form granitic intrusions under the influence of their buoyancy. The model embodies the ascent of discrete magma batches in a stepwise style by opening the fractures and then closing them after passage of the magma. In the model, magma ascends towards the subsurface via self-organized networks of rock fractures as long as the density of the surrounding rocks is greater than that of the magma. If magma rises to a zone with negative buoyancy, it stops and starts to solidify; thus forming granitic intrusions. Two fractal dimensional measures, perimeter-area (P-A) and number-area (N-A), were used to quantify the irregularity and spatial distribution of the modeled intrusions. The fractal dimension D_{AP} of P-A, as well as the fractal dimension D_P of the perimeter, show that the irregularity of the intrusions increases as the thickness of the negative buoyancy region increases. The N-A exponent D reflects the irregular size and spatial scale-invariance of the intrusions, and an abrupt inflection point occurs at an area of 100 cells, owing to the coalescence of small batches of intrusions into a larger intrusion. The scale-invariance exhibited by this system indicates that magma ascent and the formation process of granitic intrusions is a self-organized critical process and we demonstrate that a cellular automaton and fractal model is suitable for capturing, quantifying and modeling the spatial and temporal evolution of complex granitic intrusions.

1. Introduction

Magma is the molten raw material from which all igneous rocks are derived (Bowen, 1947). Understanding the processes by which magma creates solid rock is important because it is a point of beginning of the rock cycle. It has been widely observed that the vast majority of earth's magma never reaches the surface to cause an eruption (Dahm, 2000; Gudmundsson and Brenner, 2001; Pinel and Jaupart, 2004; Maccaferri et al., 2011, 2016; Rivalta et al., 2015); most of them are emplaced in the crust, and form either sills or dikes, or are assembled into plutons and laccoliths (Gudmundsson et al., 1999; Gudmundsson and Brenner, 2001; Burchardt, 2008; Gudmundsson, 2011; Menand, 2011).

The formation of granitic intrusions involves four stages, from melting (M), segregation (S), and ascent (A), to emplacement (E), spanning a huge range of geographical scales ranging from 10^{-5} m in the form of partial melting to 10^{6} m in the form of plutons and batholiths (Petford et al., 2000). Many mechanisms perform magma transport between their mid/lower crustal source region and the upper crustal emplacement levels. This process would separate the initial melt segregation into veins, followed by melt accumulation into larger volumes, and then by ascent of the magma, typically in dykes or hydrofractures, which finally lead to emplacement. The mechanisms that cover the whole MSAE process mainly consist of diapirism (Paterson and Vernon, 1995), pervasive flow (Weinberg, 1999; Brown and Solar, 1999; Collins and Sawyer, 1996), conventional dykes (Petford et al., 1993, 1994; Brown, 1994), and self-propagating hydrofractures (Weertman, 1971; Clemens and Mawer, 1992; Lister and Kerr, 1991; Dahm, 2000; Bons and van Milligen, 2001; Bons and Arnold, 2003; Bons et al., 2004). However, several studies regard diapirism as an insufficient mechanism for granitic magma ascent and emplacement (Clemens and Mawer, 1992; Vigneresse and Clemens, 2000; Petford et al., 2000). Pervasive flow typically occurs when the melt connectivity threshold is overcome,

* Corresponding author.
** Corresponding author.
E-mail addresses: zrguang@cug.edu.cn (R. Zuo), kclarke@geog.ucsb.edu (K.C. Clarke).

https://doi.org/10.1016/j.cageo.2019.05.002
Received 15 May 2018; Received in revised form 27 April 2019; Accepted 8 May 2019
Available online 10 May 2019

and an interconnected fracture network (e.g. pores, veins and dykes) is formed (Vigneresse et al., 1996; Weinberg, 1999; Vigneresse and Clemens, 2000). This mechanism for intrusion is attractive because of its ability to explain the entire MSAE process from how the smallest fractures feed into the largest dykes and subsequently feed plutons (Weinberg, 1999; Brown and Solar, 1999). However, whether a fully connected fracture network can form in reality is doubtful (Bons et al., 2004, 2009).

Research has also shown that local connectivity within a fracture network may also result in magma migration and accumulation through self-propagating hydrofractures (Weertman, 1971; Bons and van Milligen, 2001; Bons et al., 2004). Weertman (1971) presented the notion that magma could rapidly ascend within isolated hydrofractures. When the fractures filled with magma in the model exceed a critical crack length, the effective over-pressure leads to a widening of the upper tip of the fracture, which can then propagate upward owing to density differences within the magma and the surrounding rocks. Simultaneously, effective under-pressure closes the fracture at the lower tip at the same time (Weertman, 1971; Maaløe, 1987; Bons and van Milligen, 2001). After the instability leading to the propagation of the hydrofracture, magma transport in mobile hydrofractures would be stepwise and discontinuous interactions, and would aggregate with other mobile hydrofractures to promote accumulation of magma from migmatites to its final emplacement in plutons (Bons and van Milligen, 2001; Bons et al., 2004). Such stepwise transport and accumulation of magma has also been used to explain volcanic eruption activity (Scandone et al., 2007).

A conceptual model for the magmatic system, inspired by Bons et al. (2001, 2004), was developed by Scandone et al. (2007), who suggested that the storage unit of the feeding system for eruptive volcanoes is shallow discrete magma batches, instead of a deep magma chamber linked to the surface through a fully connected conduit. Individual magma batches segregated from the magma reservoir are allowed to transport in a stepwise style through self-organized crack networks by opening and then closing them after their passage.

Both analog models (Bons and van Milligen, 2001; Urtson and Soesoo, 2007, 2009) and numerical simulations (Vigneresse and Burg, 2000; Bons and van Milligen, 2001; Bon et al., 2004) have demonstrated that the distribution of melt batch volumes follows a power-law relationship. In addition, a statistical model describing magma ascent by injection of discrete batches of magma into a preformed crack network suggests that the distribution of the erupted magma volumes also exhibits a power-law relationship (Piegari et al., 2008, 2013). Volumes of leucosomes, veins, or plutons cannot typically be directly measured in the geological record, where observation is normally confined to two-dimensional outcrops, one-dimensional scan lines or drill cores. The spatial distribution of the thickness of leucosomes in migmatites (Tanner, 1999; Bons and Arnold, 2003; Bons et al., 2004; Bonamici and Duebendorfer, 2010; Hall and Kisters, 2012; Yakymchuk et al., 2013); the thickness of granites veins or dikes (Johnston and McCaffrey, 1996; Brown, 2005); pluton area distribution (Soesoo and Bons, 2015); and the length and thickness of granitic intrusions (McCaffrey and Petford, 1997; Cruden and McCaffrey, 2001; Koukouvelas et al., 2006) in the field have been documented as showing a power-law relationship. Soesoo and Bons (2015) revealed that the power law distribution exponent of leucosome widths in the migmatites and in intrusion areas in the map view are closely related to the volume-distribution exponent, which further indicates that power-law distributions of melt batches are indeed found in nature (Bons et al., 2004). As a signature of self-organized criticality (SOC, Bak et al., 1987), the widespread power-law relationships suggest that melt segregation, magma ascent and emplacement in plutons are of the SOC type from the bottom up (Brown, 2007, 2013; Soesoo and Bons, 2015). SOC is typically observed in slowly driven non-equilibrium systems with many degrees of freedom and nonlinear systematics feedbacks. SOC reflects complex system behavior, showing the property of spatial and temporal scale-invariance and is sensitive to critical thresholds where phases change, and the system seeks a new attractor (Bak et al., 1987).

As the evolution of magmatic systems is long-lasting and occurs deep in the crust, it cannot be directly observed. Numerical simulation provides an alternative research method to reproduce the process. Several numerical models based on differential equations have been constructed to further understand the ascent and emplacement of magma (Dahm, 2000; Gerya and Burg, 2007; Maccaferri et al., 2010; Keller et al., 2013; Schubert et al., 2013; Barnett and Gudmundsson, 2014; Cao et al., 2016; Gorczyk and Vogt, 2018). However, in this type of modeling method it is difficult to quantify the wide behavioral variability of complex systems (Piegari et al., 2013). A non-conventional numerical approach, cellular automata (CA) models, have proven to be powerful tools in the study of complex systems, and have been used for the simulation of transport and accumulation of magma to explain their mechanisms (Vigneresse and Burg, 2000; Bons and van Milligen, 2001). This type of CA model can describe melt transport and accumulation in partial melt systems (Vigneresse and Burg, 2000; Bons and van Milligen, 2001). However, research has yet to reproduce how magma ascent and emplacement to form granitic intrusions intuitively.

In the current study, the CA model of Piegari et al. (2013) was adopted to simulate magma ascent and the formation of granitic intrusions. As a variation of the two-dimensional (2D) Olami-Feder-Christensen (OFC) model (Olami et al., 1992), this model in geology is expressed as an abstract representation of a fault plane governed by several fracturing mechanisms, such as tectonic stress, active deformation and earthquakes (Bons et al., 2004; Piegari et al., 2013). Piegari et al. (2006, 2008) used a constant rate of stress, representing the regional and local stresses related to volcanism, to control the formation of self-organized fractures in rock. The rules linked with the OFC model were extended to magma feeding fracture systems and magma ascent under buoyancy.

However, buoyancy is closely related to the density of the surrounding rock, thus discrete magma batches move upward through self-organized crack networks only as long as the density of the surrounding rocks is greater than that of the magma fluid. If the magma rises to a zone with neutral–negative buoyancy, magma may stop and solidify, and, consequently, form intrusions in the subsurface (Piegari et al., 2013). The spatial patterns of granitic intrusions were further studied using fractal models. However, given the irregular shapes of geological structures, the thickness and length of structures are difficult to determine (McCaffrey and Petford, 1997; Wang et al., 2007). The power law relationship of the thickness and length of granitic plutons and laccoliths are typically based on the mean thickness and length. Thus, rather than discussing the power law relationship between the thickness and length of granitic intrusions, fractal measurements, i.e. the perimeter-area (P-A) (Mandelbrot, 1983; Cheng, 1995) and number-area (N-A) (Mandelbrot, 1983) fractal dimensions, were used to quantify the complexity and irregularity of intrusions.

2. Models

2.1. A cellular automaton model for magma ascent and arrest

Cellular automata can generate complex aggregate forms from only a simple set of local rules governing interactions among nearest neighbors (Wolfram, 1984). CA can overcome some of the complexities associated with solutions to the differential equations of fluid mechanics and allow different types of features to be simulated (Vigneresse and Burg, 2000; Bons and van Milligen, 2001). We started the simulation of magma ascent and arrest on a grid of $L \times L$ ($L = 120$) cells with open boundary conditions, which means that the cells of the borders of the transport region contain only three neighbors rather than four. The size of each cell was 100 m × 100 m for the 120 cells in both the horizontal and vertical directions representing a depth of 12 km. The width of the magma reservoir, which was considered filled with magma all the time, was set to $L/2$, namely 60 cells in the central part of the bottom line of the grid. We

computed statistics for over 10^8 simulations to capture data on the irregularity of the granitic intrusions after the model reached a stationary state. The state of each cell S_n ($1 < n < L^2$) was determined using three properties: $S_n = \langle e, m, \Delta\rho \rangle$, where e represents the constant rate of the stress factor controlling the formation of the fractures in the rocks; m, represents the local presence of magma in each cell; and $\Delta\rho$, represents the density contrast between the cell's magma fluid and its surrounding rocks, that control magma ascent and arrest under buoyancy. The magma is allowed to travel or rise along the connected fracture cells, and arrest occurs at the level of a neutral–negative buoyancy region in accordance with the transition rule as discussed in the following.

2.1.1. Rock fracture mechanism

The CA model for rock fracturing is based on the OFC earthquake model (Olami et al., 1992). In this model, when the stress on each spring-block exceeds the maximum static friction F_{th}, the block slips or a "fracture" occurs. In the model of Piegari et al. (2006, 2008), with a general stress field e, the ratio of the disturbing stress F to the maximum shear strength F_{th}, is defined to control the opening of a fracture. When the value of e is equal to or larger than the threshold 1, a fracture occurs. The stress field of each cell is initialized by allocating a uniformly distributed random value with $0 \leq e_i < 1$, aimed at representing the complex heterogeneity of the rocks. Then, the stress on each cell is increased at a uniform driving rate ν at each time-step (Δt)

$$e_i \rightarrow e_i + \nu\Delta t, \tag{1}$$

Where Δt denotes the elementary time-step, which is set to a 1-time unit increment.

The process continues as long as the stress in all cells is less than 1. When the stress value of any of the cells reaches 1, it fractures, and passes its stress to the nearest neighboring cells (the von Neumann 4-cell neighborhood was adopted here), as follows:

$$e_i \rightarrow 0;\ e_{nn(i)} \rightarrow e_{nn(i)} + fe_i, \tag{2}$$

where $nn(i)$ represents the von Neumann neighbor of site i, and f represents the fraction of e_i passed to its neighbors $nn(i)$.

The stress redistribution is instantaneous, and might cause the neighbors to reach a critical state, leading to further stress redistribution and fracture occurrence, until the stress value in all of the cells recovers to less than the threshold. Because several dissipative phenomena can influence the distribution of stress, a non-conservative case was considered. Thus, the isotropic and non-conservative case for stress distribution was considered with $f_{up} = f_{down} = f_{left} = f_{right} = 0.2$.

2.1.2. Magma ascent and granitic intrusion formation

The magma is allowed to rise when any cell of the transport zone is connected to the magma reservoir fractures. Similarly, the magma can intrude into the neighboring fractured sites with an upward bias caused by the buoyancy forces (Fig. 1). After the passage of individual magma batches, the fractured cells close up, and trap the magma they contain. The local presence of magma in each cell is characterized by the cell array m_i. Here, $m_i = 0$ denotes the cells with no magma, while $m_i = 1$ denotes the cells filled with magma. During the process of magma transportation, a fractured site i, with no magma, can be filled by magma derived from the reservoir or the neighboring fractured and filled cells, j. Thus, the magma field of cell i, and j can be updated as follows:

$$m_i = 0 \rightarrow m_i = 1,\ m_j = 1 \rightarrow m_j = 0, \tag{3}$$

However, the volatiles in the magma, such as dissolved water, might be lost during ascent. The value of a fractured filled cell m_i ranges from 1 to 1-n_{loss}. Here, n_{loss} is the largest percentage of gas loss, approximately 6%. The details regarding magma ascent degassing are included in Piegari et al. (2011).

During ascent, magma arrest and emplacement forms intrusions. Several mechanisms are responsible for magma arrest, such as the huge aspect ratio of dikes, the level of neutral buoyancy, and heterogeneous stress compression around the upper tip (Maccaferri et al., 2016). Among these mechanisms, the level of neutral buoyancy is the most widely studied. Maccaferri et al. (2011) showed that the rising magma arrests when it intrudes into a rock that is less dense than the magma, with the assumption that the individual magma-filled dikes are of a fixed length (Maccaferri et al., 2011). Here, we divided the cellular space into two regions (Fig. 2); a deep area with a thickness of 10 km and density $\rho_{Rdeep} = 2700\ \mathrm{kg/m^3}$, and a shallow area with a thickness of 2 km and a density $\rho_{Rshallow} = 2200\mathrm{kg/m^3}$. The density of the anhydrous magma was set to 2500 $\mathrm{kg/m^3}$ ($\rho_{magma} = 2500\mathrm{kg/m^3}$). The magma was permitted to rise through the self-organized crack network as long as the density of the surrounding rocks was greater than that of magma fluid ($\Delta\rho = \rho_R - \rho_m > 0$). If the magma rises to a zone with $\Delta\rho \leq 0$, the magmatic fluid may stop movement, start to solidify in place, and form granitic intrusions, such as dikes and sills. Because the density of the solidified magma was assumed to be greater than that of magmatic fluid with volatiles, a new region with $\Delta\rho > 0$ in the shallow zone was generated. Under this circumstance, magma can pass through the fractures in the high density region of intrusions, which eventually results in an eruption (Piegari et al., 2013). The focus of our study was to model the formation of granitic intrusions, and explore their irregularity and spatial distribution instead of describing the activity pattern of volcanoes. We restored the initial local density profiles once the granitic intrusion reached the surface; thus, a new evolution of a granitic intrusion formation process started during the next step.

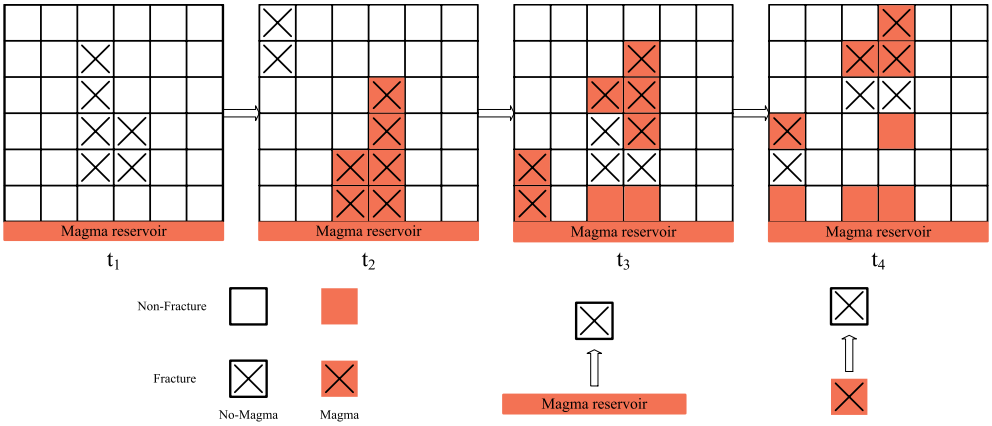

Fig. 1. Magma ascent through pre-existing fractures. Magma can only move from the reservoir to its adjacent fractured cell; or from magma filled fractured cells to an adjacent fractured cell.

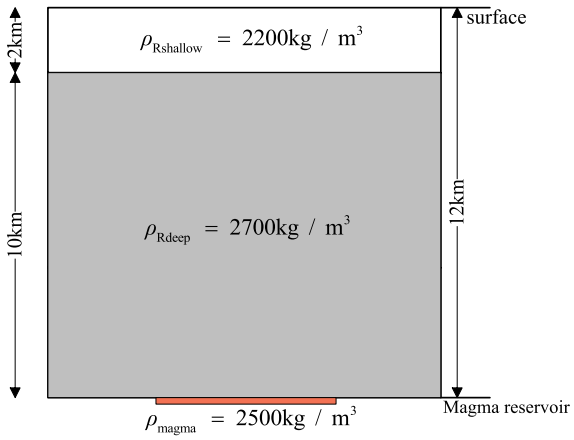

Fig. 2. The rock density profile used for the numerical simulations shown in Fig. 3.

2.2. Fractal model

2.2.1. Perimeter-area- (P-A) fractal measure

The P-A fractal dimension, proposed by Mandelbrot (1983), builds on the relationship between the perimeter (P) and area (A) within a set of irregular self-similar shaped fractals. The P-A model has been applied to describe the irregularity of the shape of rain and cloud areas (Lovejoy, 1982). A general P-A fractal model was put forward by Cheng (1995) and can be expressed as follows:

$$P \propto A^{\frac{1}{2}D_{AP}}, \tag{4}$$

where P and A represent the perimeter and area of the intrusions, respectively. D_{AP} is the P-A fractal dimension, which also can be expressed as $D_{AP} = 2D_P/D_A$, where D_P and D_A are the fractal dimensions of the perimeter and area of the intrusions, respectively. D_P and D_A can be estimated using the box-counting method (Liebovitch and Toth, 1989) as follows:

$$P(\delta) = N(\delta)\cdot\delta \propto \delta^{(1-D_P)}, \tag{5}$$

$$A(\delta) = N'(\delta)\cdot\delta^2 \propto \delta^{(2-D_A)}, \tag{6}$$

Cells with a box size δ increasing from 1, 2, 4, 8, 16, to 32 pixels were adopted to cover the intrusions and count the number of boxes ($N(\delta)$ or $N'(\delta)$) occupied by granitic intrusions. $P(\delta)$ and $A(\delta)$ are the perimeter and area of the intrusions with box size δ. The box size δ and its corresponding number $N'(\delta)$ were plotted on log-log axes to estimate the fractal dimension D_A of the granitic intrusions. The fractal dimension of the perimeter can be calculated as $D_P = \frac{1}{2}D_{AP}D_A$. The larger the value of D_P, the more irregular and branching are the granitic intrusions. The fractal dimension of D_{AP} can be estimated from the slope of the best-fitting line in the log-log plot of P versus A as follows:

$$\log P = C + \frac{1}{2}D_{AP}\log A, \tag{7}$$

The value of D_{AP} generally ranges from 1 to 2. A value of D_{AP} equal to 1 indicates regularly shaped and non-fractal geometric sets, such as squares or circles. When the value of D_{AP} increases, the shape of the granitic intrusions becomes more irregular. The perimeter varies at the same rate as the area when $D_{AP} = 2$.

2.2.2. Number-area (N-A) fractal model

The N-A fractal model can be adopted to describe the relationship between the number and area distribution of granitic intrusions using the following equation (Mandelbrot, 1983; Wang et al., 2007; Zuo et al., 2009):

$$N(\geq A) \propto A^{-D}, \tag{8}$$

where A represents the area of the intrusion, and N denotes the cumulative number of the intrusions with an area larger than, or equal to A. The exponent of D can be estimated from the slope of the best-fitting regression line of the log-log plot of $N(\geq A)$ versus A as follows:

$$\log N(\geq A) = C - D\log A, \tag{9}$$

The value of D represents the changing rate of the cumulative number of intrusions and their areas. Larger values of D indicate more intrusions of smaller area or fewer intrusions of large area.

3. Results

3.1. Magma ascent and arrest

Six images show magma ascent and arrest processes forming granitic

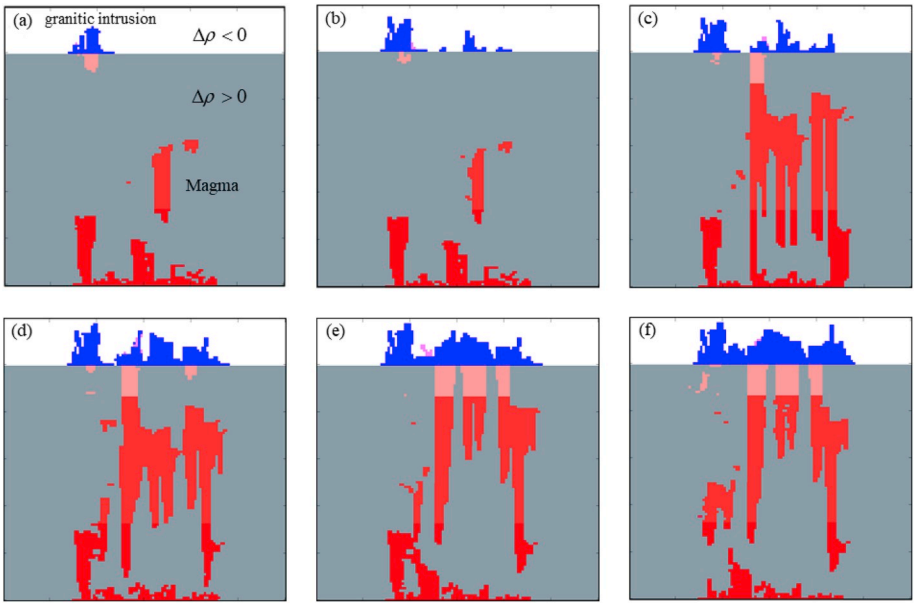

Fig. 3. A temporal CA model sequence for the evolution and formation of the granitic intrusions.

intrusions in the shallow zone (Fig. 3). The magma, with red cells, first ascends through the fractures (not visible) in the region where $\Delta\rho > 0$ (gray cells). The volatiles in the magma might be lost during the ascent, and the colors of the cells ranging from red to magenta represent the degassing degree (Piegari et al., 2011). When magma rises to the region where $\Delta\rho \leq 0$ (white cells), it stops and solidifies, and a higher density profile ($\Delta\rho > 0$) in the shallow region is generated which changes the red region to blue as shown in the image. Thus, the uniform layer of rock density varies in a non-trivial manner. The newly rising magma can, in turn, ascend through the fracture cells in the formed intrusions (blue region). This type of positive and negative feedback of density profile promotes the growth and formation of granitic intrusions which emerge as complex irregular fractal-like shapes. We noticed that a CA model with only a set of local rules can simulate the complex process that generates self-organized fractures, magma ascent, dike formation, and volcanic eruptions.

3.2. Irregularity analysis of granitic intrusions

The fractal dimension D_A of an area was estimated via box counting. Six squares with a box size δ ranging from 1, 2, 4, 8, 16, to 32 pixels were used to cover the intrusion region, and the number of the boxes ($N'(\delta)$) covered by the blue region in the image was counted. The box size δ and its corresponding number of boxes $N'(\delta)$ were plotted on a log-log graph to estimate the fractal dimension D_A (Fig. 4). The fractal dimension D_A of the intrusion area can be calculated from the negative slope of the line of best fit. The value of D_A ($1.79 < 2$) indicates that the intrusions are irregular and show a fractal area.

The perimeters and areas of the intrusions were plotted on log-log graphs and the exponent D_{AP} estimated from the slope of the linear regression (Fig. 5). The relatively high correlation coefficient R^2 (0.99) indicates that the perimeter and area follow a power-law relationship, and it is also a strong indicator of scale invariance or a fractal nature. The slope coefficient is 0.64, and the corresponding D_{AP} value is 1.28, implying the granitic intrusions have an irregular shape. The corresponding fractal dimensional of the perimeter (D_P) is 1.15, according to the formula $D_P = \frac{1}{2} D_{AP} D_A$, which reflects the winding nature of the intrusion boundary.

The area of the granitic intrusions (A) and the cumulative number of the intrusions with an area larger than or equal to A plotted on the log-log graph shows a broadly concave downward curve (Fig. 6). The curve can be decomposed into two segments with an abrupt inflection point between them (Fig. 6). Areas less than 100 cells exhibit a rather flat power law distribution with a scaling exponent equal to 0.32, while areas larger than 100 exhibit a steeper power law distribution with a scaling exponent equal to 1.70. This kind of concave downward curve is widespread in power-law distributions of leucosome thickness and intrusions areas (Bons and Arnold, 2003; Bons et al., 2004; Koukouvelas et al., 2006; Bonamici and Duebendorfer, 2010; Hall and Kisters, 2012; Yakymchuk et al., 2013; Soesoo and Bons, 2015). Reasons for the break of slope might be attributed to undersampling of the smaller thicknesses (either still fully buried or completely eroded away) or a natural characteristic of the pluton population (Bons et al., 2004; Koukouvelas et al., 2006; Yakymchuk et al., 2013; Soesoo and Bons, 2015). The missing of small intrusions did not occur when counting cells for our simulation results. Thus, we attribute the abrupt inflection point to the small batch intrusions coalescing into larger intrusions as the granitic intrusions accumulate in a stepwise style. The evolution of the area of the granitic intrusions (Fig. 7) shows that the area drastically increases at a certain time, and the increase is instantaneous. This increase in intrusion area occurs when the magma ascends to a rock region that is less dense than that of the magma. The system spends most of its time on the formation of self-organized cracks, and during the magma ascent in the deep region with a density greater than that of the magma.

The effects of the thickness of the neutral-negative buoyancy zone on the formation of intrusions was further studied by varying the thickness of the neutral-negative buoyancy zone (the shallowest zone) from 2 km

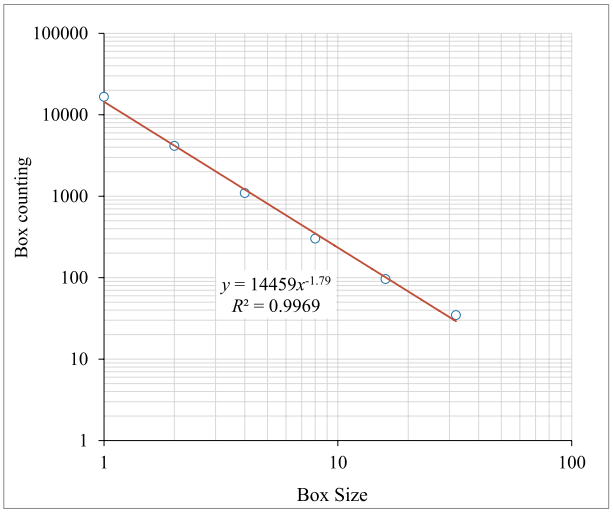

Fig. 4. Log-log axes of Number-Size model for fractal dimensional of areas.

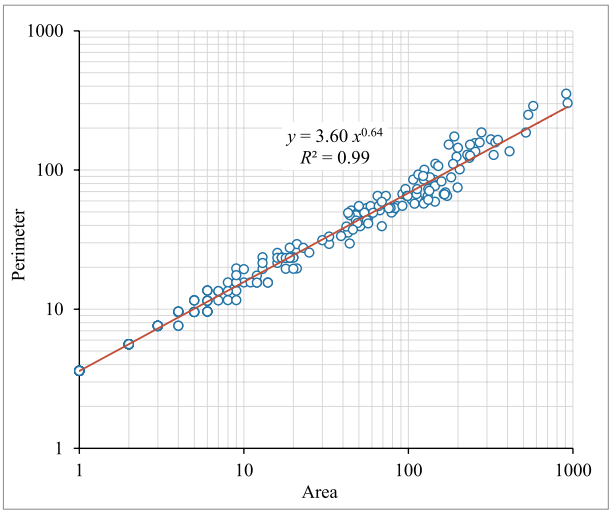

Fig. 5. Log-log axes of Area-perimeter of the granitic intrusions.

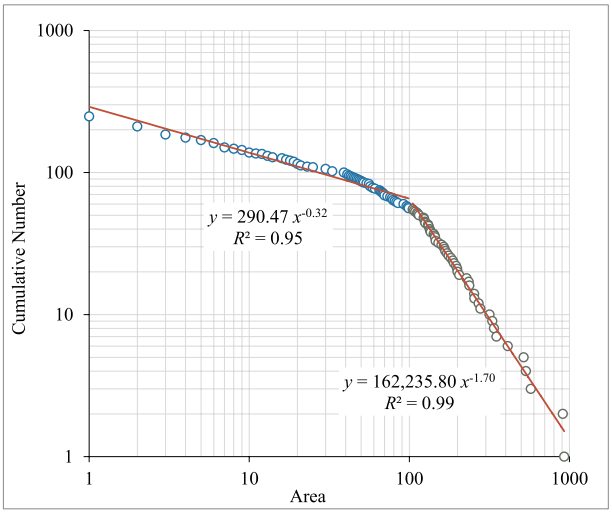

Fig. 6. Log-log axes of Cumulative Number-Area of the granitic intrusions.

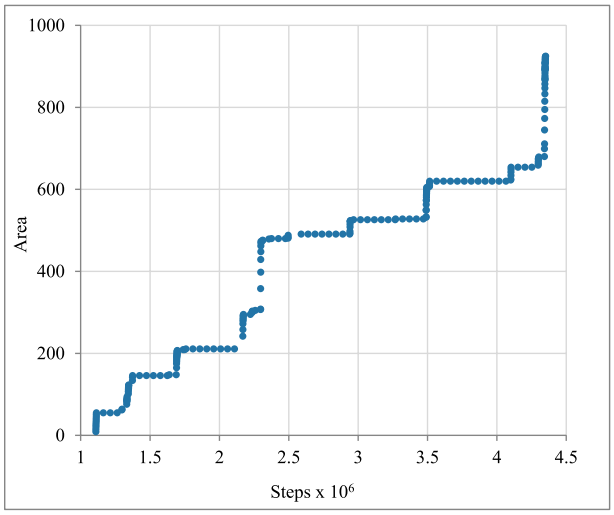

Fig. 7. Time line of the evolution of granitic intrusions area.

to 5 km, with the thickness of the deep region simultaneously reduced from 10 km to 7 km. The simulated results displayed in Fig. 8 show that a power law relationship exists between the perimeter and area of the intrusions across the different thicknesses, as all of the correlation coefficients R^2 are significant and greater than 0.9 (Fig. 8). The slope varied from 0.64 to 0.67, and the corresponding D_{AP} varied from 1.28 to 1.34. The box size and the corresponding number of boxes shown in Fig. 9 produced perfectly fitting lines on the log-log graph, indicating complete scale-invariance in the area of the intrusions. The fractal dimension D_A of the area, as the negative slope of the best-fitting straight line, varied from 1.79, 1.82, 1.83 to 1.85, indicating that the intrusions formed with different thicknesses show similar fractal areas. The corresponding fractal dimensions D_P of the perimeter were 1.15, 1.22, 1.23 and 1.24. The fractal dimensions of D_P show a trend of growth in general, which indicates that the irregularity or complexity of the intrusions gradually increases with an increase in the thickness of the shallow region.

The results of the area and the cumulative number of intrusions in different thicknesses of the neutral-negative buoyancy zone show similar downward concavity curves compared to those of Fig. 6. The abrupt inflection points between them divide the curves into two segments (Fig. 10). The transition occurs at or near an area of 100 cells with a different thickness of the neutral-negative buoyancy zone ranging from 2 km to 5 km. The relationships between the area and cumulative number also follow power law distributions for the different segments in these four different thicknesses. With the increase of the thicknesses of the shallow region, the fractal dimensions of D decrease from 0.32, 0.29, 0.27 to 0.23 in areas less than 100, and decrease from 1.70, 1.23, 1.20 and 1.09 in areas larger than 100. The fractal dimensions of D monotonically decrease at two segments, respectively, indicating that fewer small intrusions or more large intrusions formed with the increase in the thickness of the neutral-negative buoyancy zone.

4. Discussion

The magma ascent mechanism in this study is motivated from that of Bons et al. (2001, 2004). Both models favor stepwise ascent and accumulation of individual magma batches through pre-existing fractures rather than fully interconnected fracture networks (Bons et al., 2004, 2009; Scandone et al., 2007). In the model of Bons et al. (2001, 2004), the magma-filled hydrofractures move upward when the effective normal stress gradient along the fractures exceeds a critical crack length. The stress gradient density difference between the magma and surrounding rock is determined by new magma intrusion into the reservoir,

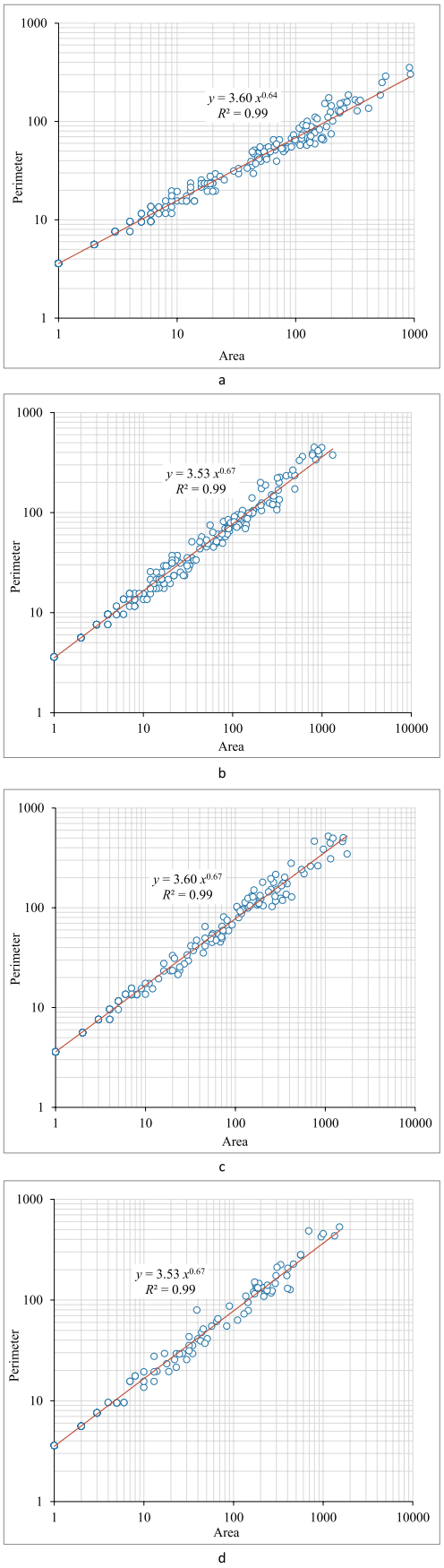

Fig. 8. Log-log axes of Perimeter-Area of the granitic intrusions for the thickness of the negative region (a)2 km, (b)3 km, (c)4 km, and (d)5 km.

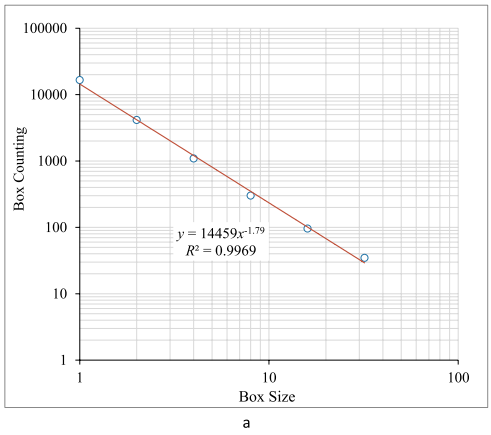

a

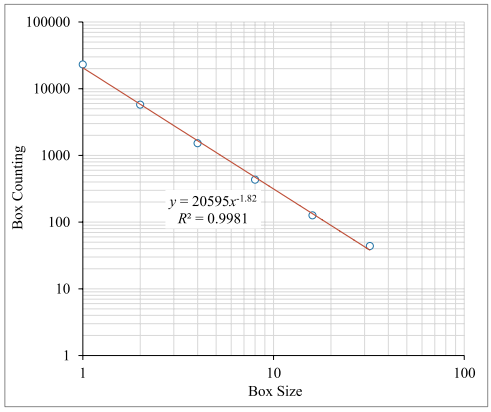

b

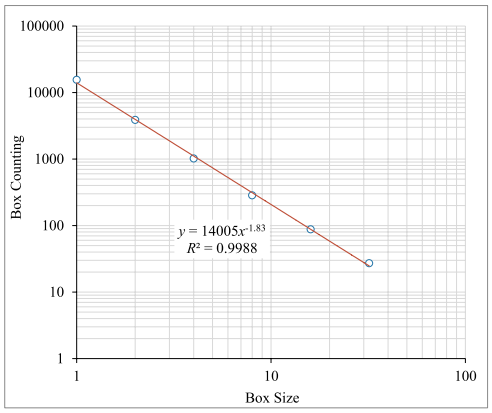

c

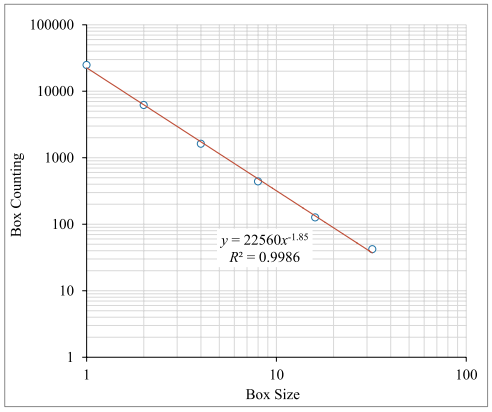

d

Fig. 9. Log-log axes of Number-Size model for fractal dimensional of areas for the thickness of the negative region (a) 2 km, (b) 3 km, (c) 4 km, and (d) 5 km.

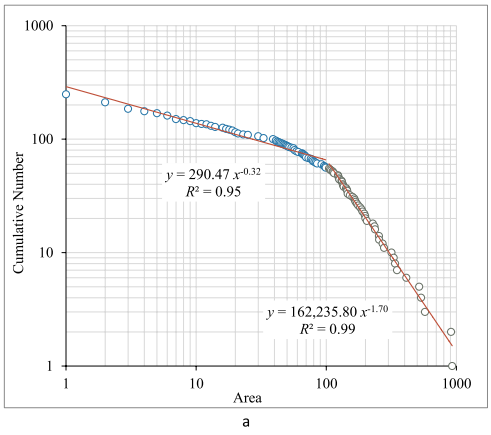

a

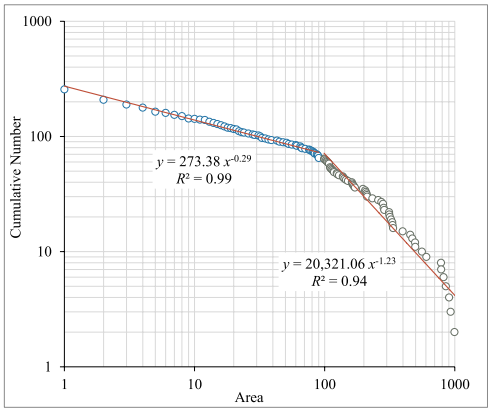

b

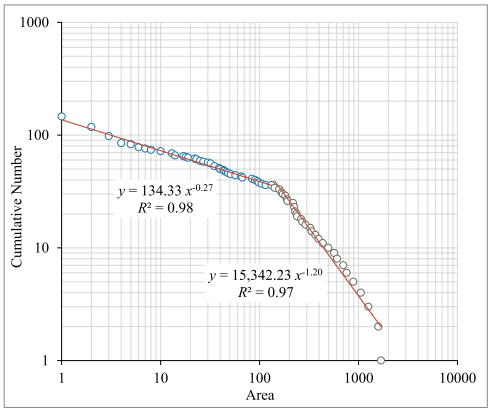

c

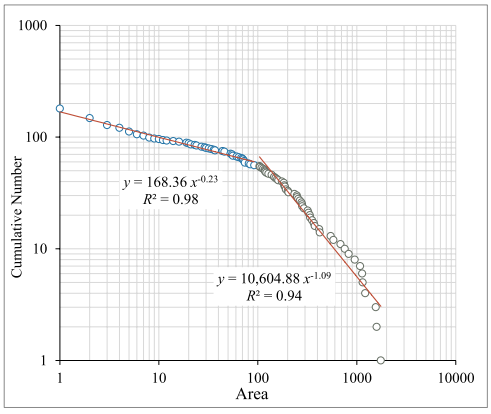

d

Fig. 10. Log-log axes of cumulative number-area of the granitic intrusions for the thickness of the negative region (a) 2 km, (b) 3 km, (c) 4 km, and (d) 5 km.

deformation or tectonic stress, earthquakes and their concurrent effects (Clemens and Mawer, 1992; Rubin, 1998; Bons et al., 2004; Butters et al., 2017). However, in this study, the dynamic stress was independent of the magma field (Piegari et al., 2008, 2013). The constant rate stress, which represents the regional and local stresses, controls the formation of self-organized fractures in the rocks. The buoyancy generated by the density difference between the magma and the surrounding rock controls magma migration in the open fractures. The aim of this assumption was to capture key features of the fracture field to reproduce how magma ascent and emplacement occur, rather than to identify the main causes of fracturing. Various studies have shown that stress induced fracture networks are a SOC process (Chen et al., 1991; Olami et al., 1992; Piegari et al., 2008, 2013). Six images in a temporal sequence show the processes by which the magma ascends and forms granitic intrusions using the CA model. A couple of rules and properties linked with the OFC model reproduce the discrete magma batches ascent in a stepwise style through self-organized crack networks by allowing the ascent of individual magma batches by opening and then closing cracks upon their passage, during which the closure mechanism is different from that of Bons et al. (2001, 2004). We noticed that the ascending magma stops and granitic intrusions start to form because of the effect of the negative buoyancy. The granitic intrusions change the density profiles, which have positive or negative feedbacks on magma ascent and granitic accumulation. The less dense region may prevent magma ascent (negative feedback), and result in forming granitic intrusions (higher density region) to allow magma ascent again (positive feedback). The positive/negative feedbacks can overcome the density barrier effect of the buoyant ascent of the magmas, further explaining why multiple dikes or granitic intrusions can pass through rocks with a density lower than that of the anhydrous magma in field observations (Zollo et al., 1996; Di Maio et al., 1998).

The instantaneous increase in intrusion area occurs when the magma intrudes into the fractured rock that is less dense than the magma, when an “avalanche” occurs. In addition, as the end products of the “avalanche”, the granitic intrusions can be modeled by the fractal models (P-A and N-A), which suggests that the distribution of the frequency-size and shape irregularity show a power law (scale-invariant) relationship. The previous experiments and numerical modeling results suggest that the distribution of magma batch volumes can be described by a power law relationship resulting from a stepwise transport and accumulation. However, volumes of leucosomes, veins, or plutons cannot typically be directly measured in the geological record, where observation is normally confined to two-dimensional outcrops, one-dimensional scan lines or drill cores. By adopting a vertical slice along a transect in the CA model, the power law distribution of granitic intrusions areas under the surface can further support the assertion that magma ascent and granitic intrusion formation processes are SOC (Brown, 2007, 2013; Soesoo and Bons, 2015). We present a few more points regarding the development and evolution of magma transport system before considering a specific case history. The model provides a near-perfect expression for the generation of a crack network and reproduces the processes of magma ascent and formation of granitic intrusions; the fractal model can efficiently quantify this type of irregularity in the objects.

However, the model is relatively idealized, because it only considers the effects of density on the magma ascent. The viscosity of the magma, rigidity discontinuity, fracture toughness heterogeneity, and external stress field play important roles in magma ascent and arrest (Brown, 1994; Petford et al., 2000; Maccaferri et al., 2010, 2011; 2016; Rivalta et al., 2015). For example, the propagated dikes would stop without deviating when they propagate in the direction of a topographic load with a low overpressure at the upper tip or when they intrude into a layer where they become neutrally or negatively buoyant (Maccaferri et al., 2011). Both these factors are necessary for a cellular automaton model to accurately reproduce the real geological process of magma ascent and arrest.

5. Conclusions

Even if the distributions of the event sizes themselves are important, our view of nature is mostly based on our understanding of the processes that generate the patterns we observe in the field. In this study, we used a cellular automaton to reproduce magma ascent and the formation of granitic intrusions intuitively. In the model, magma is allowed to rise along the preformed fractures in a stepwise style by opening and then closing after their passage; magma stops rising at the neutral–negative buoyancy region, then forms granitic intrusions. The model does a good job of replicating the growth process of granitic intrusions under the positive and negative feedbacks of rock density profiles. Statistical data analysis of the distribution of perimeter and area, frequency and cumulative area of granitic intrusions towards the non-linear characteristic of scale-invariance indicating that the magma ascent and granitic intrusion formation processes are SOC processes, which further support the assertion that granitic ascent and emplacement are also self-organized critical phenomena. In conclusion, a cellular automaton is a helpful tool to link the fracturing mechanism and rock or magma density to magma ascent and emplacement processes that may both predict and explain the complex processes in nature and causes of self-organization.

Author contributions

Yihui Xiong, Renguang Zuo and Keith C. Clarke designed and carried out this study. Yihui Xiong implemented the model and wrote the paper. Renguang Zuo and Keith C. Clarke revised the paper and provided valuable advice.

Acknowledgements

This research was supported by the National Natural Science Foundation of China (No. 41772344), and MOST Special Fund from the State Key Laboratory of Geological Processes and Mineral Resources, China University of Geosciences (MSFGPMR03-3). Also, the first author gratefully acknowledges the financial support from China Scholarship Council (No. 201706410020) for support as a joint-education PhD student in the Department of Geography, University of California, Santa Barbara.

References

Bak, P., Tang, C., Wiesenfeld, K., 1987. Self-organized criticality: an explanation of the 1/f noise. Phys. Rev. Lett. 59, 381–384.
Barnett, Z.A., Gudmundsson, A., 2014. Numerical modelling of dykes deflected into sills to form a magma chamber. J. Volcanol. Geotherm. Res. 281, 1–11.
Bonamici, C.E., Duebendorfer, E.M., 2010. Scale-invariance and self-organized criticality in migmatites of the southern Hualapai Mountains, Arizona. J. Struct. Geol. 32, 1114–1124.
Bons, P.D., van Milligen, B.P., 2001. New experiment to model self-organized critical transport and accumulation of melt and hydrocarbons from their source rocks. Geology 29, 919–922.
Bons, P.D., Dougherty-Page, J., Elburg, M.A., 2001. Stepwise accumulation and ascent of magmas. J. Metamorph. Geol. 19, 627–633.
Bons, P.D., Arnold, J., 2003. Accumulation and self-organization in hydrofracture transport of fluids. J. Geochem. Explor. 78, 667–670.
Bons, P.D., Arnold, J., Elburg, M.A., Kalda, J., Soesoo, A., van Milligen, B.P., 2004. Melt extraction and accumulation from partially molten rocks. Lithos 78, 25–42.
Bons, P.D., Becker, J.K., Elburg, M.A., Urtson, K., 2009. Granite formation: stepwise accumulation of melt or connected networks? Earth and Environmental Science Transactions of the Royal Society of Edinburgh 100, 105–115.
Bowen, N.L., 1947. Magmas. Geol. Soc. Am. Bull. 58, 263–280.
Brown, M., 1994. The generation, segregation, ascent and emplacement of granite magma: the migmatite-to-crustally-derived granite connection in thickened orogens. Earth Sci. Rev. 36, 83–130.
Brown, M., Solar, G.S., 1999. The mechanism of ascent and emplacement of granite magma during transpression: a syntectonic granite paradigm. Tectonophysics 312, 1–33.
Brown, M., 2005. Synergistic Effects of Melting and Deformation: an Example from the Variscan Belt, Western France, vol. 243. Geological Society, London, Special Publications, pp. 205–226.
Brown, M., 2007. Crustal melting and melt extraction, ascent and emplacement in orogens: mechanisms and consequences. J. Geol. Soc. 164, 709–730.

Brown, M., 2013. Granite: from genesis to emplacement. Geol. Soc. Am. Bull. 125, 1079–1113.
Burchardt, S., 2008. New insights into the mechanics of sill emplacement provided by field observations of the Njardvik Sill, Northeast Iceland. J. Volcanol. Geotherm. Res. 173, 280–288.
Butters, O.J., Sarson, G.R., Bushby, P.J., 2017. Effects of magma-induced stress within a cellular automaton model of volcanism. J. Volcanol. Geotherm. Res. 341, 94–103.
Cao, W., Kaus, B.J., Paterson, S., 2016. Intrusion of granitic magma into the continental crust facilitated by magma pulsing and dike-diapir interactions: numerical simulations. Tectonics 35, 1575–1594.
Chen, K., Bak, P., Obukhov, S.P., 1991. Self-organized criticality in a crack-propagation model of earthquakes. Phys. Rev. 43, 625–629.
Cheng, Q., 1995. The perimeter-area fractal model and its application to geology. Math. Geol. 27, 69–82.
Clemens, J.D., Mawer, C.K., 1992. Granitic magma transport by fracture propagation. Tectonophysics 204, 339–360.
Collins, W.J., Sawyer, E.W., 1996. Pervasive granitoid magma transfer through the lower–middle crust during non-coaxial compressional deformation. J. Metamorph. Geol. 14, 565–579.
Cruden, A.R., McCaffrey, K.J.W., 2001. Growth of plutons by floor subsidence: implications for rates of emplacement, intrusion spacing and melt-extraction mechanisms. Phys. Chem. Earth Solid Earth Geodes. 26, 303–315.
Dahm, T., 2000. Numerical simulations of the propagation path and the arrest of fluid-filled fractures in the Earth. Geophys. J. Int. 141, 623–638.
Di Maio, R., Mauriello, P., Patella, D., Petrillo, Z., Piscitelli, S., Siniscalchi, A., 1998. Electric and electromagnetic outline of the Mount Somma–Vesuvius structural setting. J. Volcanol. Geotherm. Res. 82, 219–238.
Gerya, T.V., Burg, J.P., 2007. Intrusion of ultramafic magmatic bodies into the continental crust: numerical simulation. Phys. Earth Planet. In. 160, 124–142.
Gorczyk, W., Vogt, K., 2018. Intrusion of magmatic bodies into the continental crust: 3-D numerical models. Tectonics 37, 705–723.
Gudmundsson, A., Marinoni, L.B., Marti, J., 1999. Injection and arrest of dykes: implications for volcanic hazards. J. Volcanol. Geotherm. Res. 88, 1–13.
Gudmundsson, A., Brenner, S.L., 2001. How hydrofractures become arrested. Terra. Nova 13, 456–462.
Gudmundsson, A., 2011. Deflection of dykes into sills at discontinuities and magma-chamber formation. Tectonophysics 500, 50–64.
Hall, D., Kisters, A., 2012. The stabilization of self-organised leucogranite networks—implications for melt segregation and far-field melt transfer in the continental crust. Earth Planet. Sci. Lett. 355, 1–12.
Johnston, J.D., McCaffrey, K.J.W., 1996. Fractal geometries of vein systems and the variation of scaling relationships with mechanism. J. Struct. Geol. 18, 349–358.
Keller, T., May, D.A., Kaus, B.J., 2013. Numerical modelling of magma dynamics coupled to tectonic deformation of lithosphere and crust. Geophys. J. Int. 195, 1406–1442.
Koukouvelas, I.K., Pe-Piper, G., Piper, D.J., 2006. The relationship between length and width of plutons within the crustal-scale Cobequid Shear Zone, northern Appalachians, Canada. Int. J. Earth Sci. 95, 963–976.
Liebovitch, L.S., Toth, T., 1989. A fast algorithm to determine fractal dimensions by box counting. Phys. Lett. 141, 386–390.
Lister, J.R., Kerr, R.C., 1991. Fluid-mechanical models of crack propagation and their application to magma transport in dykes. J. Geophys. Res.: Solid Earth 96, 10049–10077.
Lovejoy, S., 1982. Area-perimeter relation for rain and cloud areas. Science 216, 185–187.
Maaløe, S., 1987. The generation and shape of feeder dykes from mantle sources. Contrib. Mineral. Petrol. 96, 47–55.
Maccaferri, F., Bonafede, M., Rivalta, E., 2010. A numerical model of dyke propagation in layered elastic media. Geophys. J. Int. 180, 1107–1123.
Maccaferri, F., Bonafede, M., Rivalta, E., 2011. A quantitative study of the mechanisms governing dike propagation, dike arrest and sill formation. J. Volcanol. Geotherm. Res. 208, 39–50.
Maccaferri, F., Rivalta, E., Passarelli, L., Aoki, Y., 2016. On the mechanisms governing dike arrest: insight from the 2000 Miyakejima dike injection. Earth Planet. Sci. Lett. 434, 64–74.
Mandelbrot, B.B., 1983. The Fractal Geometry of Nature, vol. 173. WH freeman, New York.
McCaffrey, K.J.W., Petford, N., 1997. Are granitic intrusions scale invariant? J. Geol. Soc. 154, 1–4.
Menand, T., 2011. Physical controls and depth of emplacement of igneous bodies: a review. Tectonophysics 500, 11–19.
Olami, Z., Feder, H.J.S., Christensen, K., 1992. Self-organized criticality in a continuous, non-conservative cellular automaton modeling earthquakes. Phys. Rev. Lett. 68, 1244–1248.
Paterson, S.R., Vernon, R.H., 1995. Bursting the bubble of ballooning plutons: a return to nested diapirs emplaced by multiple processes. Geol. Soc. Am. Bull. 107, 1356–1380.
Petford, N., Kerr, R.C., Lister, J.R., 1993. Dike transport of granitoid magmas. Geology 21, 845–848.
Petford, N., Lister, J.R., Kerr, R.C., 1994. The ascent of felsic magmas in dykes. Lithos 32, 161–168.
Petford, N., Cruden, A.R., McCaffrey, K.J.W., Vigneresse, J.L., 2000. Granite magma formation, transport and emplacement in the Earth's crust. Nature 408, 669–673.
Piegari, E., Cataudella, V., Di Maio, R., Milano, L., Nicodemi, M., 2006. A cellular automaton for the factor of safety field in landslides modeling. Geophys. Res. Lett. 33, L01403. https://doi.org/10.1029/2005GL024759.
Piegari, E., Cataudella, V., Di Maio, R., Milano, L., Nicodemi, M., Scandone, R., 2008. A model of volcanic magma transport by fracturing stress mechanisms. Geophys. Res. Lett. 35, L06308. https://doi.org/10.1029/2007GL032710.
Piegari, E., Di Maio, R., Scandone, R., Milano, L., 2011. A cellular automaton model for magma ascent: degassing and styles of volcanic eruptions. J. Volcanol. Geotherm. Res. 202, 22–28.
Piegari, E., Di Maio, R., Scandone, R., 2013. Analysis of the activity pattern of volcanoes through self-organized crack networks: the effect of density barriers—an application to Vesuvius activity in the period 1631–1944. Earth Planet. Sci. Lett. 371, 269–277.
Pinel, V., Jaupart, C., 2004. Magma storage and horizontal dyke injection beneath a volcanic edifice. Earth Planet. Sci. Lett. 221, 245–262.
Rivalta, E., Taisne, B., Bunger, A.P., Katz, R.F., 2015. A review of mechanical models of dike propagation: schools of thought, results and future directions. Tectonophysics 638, 1–42.
Rubin, A.M., 1998. Dike ascent in partially molten rock. J. Geophys. Res.: Solid Earth 103, 20901–20919.
Scandone, R., Cashman, K.V., Malone, S.D., 2007. Magma supply, magma ascent and the style of volcanic eruptions. Earth Planet. Sci. Lett. 253, 513–529.
Schubert, M., Driesner, T., Gerya, T.V., Ulmer, P., 2013. Mafic injection as a trigger for felsic magmatism: a numerical study. Geochem. Geophys. Geosyst. 14, 1910–1928.
Soesoo, A., Bons, P.D., 2015. From migmatites to plutons: power law relationships in the evolution of magmatic bodies. Pure Appl. Geophys. 172, 1787–1801.
Tanner, D.C., 1999. The scale-invariant nature of migmatite from the Oberpfalz, NE Bavaria and its significance for melt transport. Tectonophysics 302, 297–305.
Urtson, K., Soesoo, A., 2007. An analogue model of melt segregation and accumulation processes in the Earth's crust. Est. J. Earth Sci. 56, 3–10.
Urtson, K., Soesoo, A., 2009. Stepwise magma migration and accumulation processes and their effect on extracted melt chemistry. Est. J. Earth Sci. 58, 246–258.
Vigneresse, J.L., Barbey, P., Cuney, M., 1996. Rheological transitions during partial melting and crystallization with application to felsic magma segregation and transfer. J. Petrol. 37, 1579–1600.
Vigneresse, J.L., Clemens, J.D., 2000. Granitic Magma Ascent and Emplacement: Neither Diapirism Nor Neutral Buoyancy, vol. 174. Geological Society, London, Special Publications, pp. 1–19.
Vigneresse, J.L., Burg, J.P., 2000. Continuous vs. discontinuous melt segregation in migmatites: insights from a cellular automaton model. Terra. Nova 12, 188–192.
Wang, Z., Cheng, Q., Cao, L., Xia, Q., Chen, Z., 2007. Fractal modelling of the microstructure property of quartz mylonite during deformation process. Math. Geol. 39, 53–68.
Weertman, J., 1971. Theory of water-filled crevasses in glaciers applied to vertical magma transport beneath oceanic ridges. J. Geophys. Res. 76, 1171–1183.
Weinberg, R.F., 1999. Mesoscale pervasive felsic magma migration: alternatives to dyking. Lithos 46, 393–410.
Wolfram, S., 1984. Cellular automata as models of complexity. Nature 311, 419–424.
Yakymchuk, C., Brown, M., Ivanic, T.J., Korhonen, F.J., 2013. Leucosome distribution in migmatitic paragneisses and orthogneisses: a record of self-organized melt migration and entrapment in a heterogeneous partially-molten crust. Tectonophysics 603, 136–154.
Zollo, A.E.A., Gasparini, P., Virieux, J., Le Meur, H., De Natale, G., Biella, G., Boschi, E., Capuano, P., de Franco, R., dell' Aversana, P., De Matteis, R., Guerra, I., Iannaccone, G., Mirabile, L., Vilardo, G., 1996. Seismic evidence for a low-velocity zone in the upper crust beneath Mount Vesuvius. Science 274, 592–594.
Zuo, R., Cheng, Q., Xia, Q., Agterberg, F.P., 2009. Application of fractal models to distinguish between different mineral phases. Math. Geosci. 41, 71–80.